Hydrol. Earth Syst. Sci. Discuss., 10, 6153–6192, 2013
www.hydrol-earth-syst-sci-discuss.net/10/6153/2013/
doi:10.5194/hessd-10-6153-2013

Hydrology and Earth System Sciences
Open Access
Discussions

Modeling regional evaporation through ANFIS incorporated solely with remote sensing data

F.-J. Chang and W. Sun

Department of Bioenvironmental Systems Engineering, National Taiwan University, No. 1, Sec. 4, Roosevelt Road, Da-An District, Taipei, 10617, Taiwan

Received: 22 April 2013 – Accepted: 30 April 2013 – Published: 16 May 2013

Correspondence to: F.-J. Chang (changfj@ntu.edu.tw)

Published by Copernicus Publications on behalf of the European Geosciences Union.

Abstract

The study aims to model regional evaporation that possesses the ability to present the spatial distribution of evaporation across the whole Taiwan by the adaptive network-based fuzzy inference system (ANFIS) based solely on remote sensing data. The remote sensing data used in this study consist of Landsat image products including Enhanced Vegetation Index (EVI) and land surface temperature (LST). The model construction is designed through two types of data allocation (temporal and spatial) driven with the same ten-year data of EVI and LST derived from Landsat images. Evidences indicate the estimation model based solely on remotely sensed data can effectively detect the spatial variation of evaporation and appropriately capture the evaporation trend with acceptable errors of about 1 mm day^{-1}. The results also demonstrate the composite of EVI and LST input to the proposed estimation model improves the accuracy of estimated evaporation values as compared with the model using LST as the only input, which reveals EVI indeed benefits the estimation process. The results suggest Model-T (temporal input allocation) is suitable for making island-wide evaporation estimation while Model-S (spatial input allocation) is suitable for making evaporation estimation at ungauged sites. An island-wide evaporation map for the whole study area (Taiwan Island) is then derived. It concludes the proposed ANFIS model incorporated solely with remote sensing data can reasonably well generate evaporation estimation and is reliable as well as easily applicable for operational estimation of evaporation over large areas where the network of ground-based meteorological gauging stations is not dense enough or readily available.

1 Introduction

Land surface evaporation is an essential component of the hydrological cycle and a significant implication in the management of water resources and agricultural irrigation. However measurement of evaporation with accuracy is a difficult task. The complex

HESSD
10, 6153–6192, 2013

interactions between land and atmosphere systems hinder effective and accurate estimations of evaporation. The amount of evaporation is affected by various meteorological factors such as temperature, solar radiation and wind speed. Researchers attempted to estimate evaporation by fitting the linear relationship between meteorological factors (Coulomb et al., 2001). Donohue et al. (2010) detected the dynamics in evaporation within variable climate conditions using various evaporation formulations. The need for accurate estimates of evaporation has been raised (Chang et al., 2013). Methods of evaporation estimation were implemented mainly with ground-based observations, which achieved different degrees of success (Blyth and Harding, 2011). However the accuracy of estimation highly relies on precise and reliable meteorological data measured locally, and the constructed models are commonly subject to rigorous local calibrations so that have limited global availability. Moreover, it is impractical to estimate evaporation over large areas using surface meteorological parameters. Due to these limitations, conventional regression modeling techniques and ground-based observation networks need to be further refined to effectively improve estimation performance by adopting advanced techniques, such as artificial neural networks, with the global coverage of remotely sensed hydro-meteorological data.

Artificial neural networks (ANNs) are capable of identifying complex nonlinear relationships between input and output data sets and have been recognized as effective tools to model nonlinear systems, particularly for problems in which the characteristics of operation processes are difficult to describe by physical equations. ANNs have been extensively explored for their applicability and reliability in various hydrosystem problems (Abrahart et al., 2012; Chen and Chang, 2009; Chiang and Chang, 2009). Besides, a large number of researchers have satisfactorily applied ANNs to the estimation of evaporation and/or evapotranspiration based mainly on ground-based hydro-meteorological data (Chung et al., 2012; Chang et al., 2010; Kim and Kim, 2008; Landeras et al., 2008; Parasuraman et al., 2007; Shiri and Kisi, 2011; Sudheer et al., 2002).

HESSD
10, 6153–6192, 2013

Satellite remote sensing techniques can provide an unprecedented global coverage of hydrological information that is neither easy nor cost-effective to collect through ground-based measurement (Sims et al., 2008; Sucksdorff and Ottle, 1990). The techniques are extensively investigated by a series of modeling schemes with varying degrees of complexity and are implemented in diverse hydrosystem domains, such as surface parameters (Matsushita and Fukushima, 2009), heat flux (Cammalleri et al., 2010), soil moisture (Liu et al., 2009; Wang et al., 2011), daily evapotranspiration (Anderson et al., 2011; Cristóbal et al., 2011) and water consumption (Contreras et al., 2011). Remote sensing techniques, however, cannot readily provide atmospheric observations such as wind speed, humidity, air temperature and vapor pressure that are necessary components for estimating evaporation over large heterogeneous areas. Consequently, many hydro-meteorologists proposed the combined use of remote sensing observations and ancillary surface as well as atmospheric observations (Farah and Bastiaanssen, 2011; Glenn et. al., 2011). Jiang and Islam (2001) estimated surface evaporation over large areas based on an extension of the Priestley–Taylor equation and a relationship between remotely sensed surface temperature and vegetation index. Rivas and Caselles (2004) used remote sensing-based surface temperature and local meteorological data to estimate spatial reference evaporation.

Due to mountainous terrains and steep river morphology, the uneven distribution of water resources and evaporation has resulted in a number of challenging tasks in Taiwan, especially in the management of agricultural irrigation, terrestrial water balance, water supply, and land resources planning. For estimating the surface evaporation map across the whole Taiwan, this study intends to develop a robust and operational neuro-fuzzy network model by sole use of simply Landsat satellite imagery products including enhanced vegetation index (EVI) and land surface temperature (LST) as model inputs, without locally measured meteorological data. The proposed method is expected to effectively deliver an island-wide evaporation map with reasonable accuracy and substantially reduce the possible cost of manpower and measurements involved in ground-based models.

HESSD
10, 6153–6192, 2013

2 Methodologies

The main objective of this study was to estimate evaporation and produce an island-wide evaporation map compiled entirely from remote sensing data by using the adaptive network-based fuzzy inference system (ANFIS). The remote sensing data of EVI and LST for use were derived from Landsat Enhanced Thematic Mapper (ETM+) and Thematic Mapper (TM) satellite imagery. The merits of methodologies used in this study are briefly addressed as follows.

2.1 ANFIS

The fuzzy logic theories are based on the way how brains deal with inexact information, while artificial neural networks (ANNs) have an effective ability to learn, to self-organize its structure, and to adapt the parameters in an interactive manner. The inspiration and strength of these two methods are different, where ANNs offer good performance in handling sensory data while fuzzy inference models often deal with issues such as reasoning at a higher analytical level than ANNs. Thus, a promising approach to capturing the strengths and benefits of both a fuzzy model and an ANN is to merge them into a hybrid system with a single framework. The ANFIS proposed by Jang (1993) is an integrated algorithm inherited with the mighty ability of a fuzzy system and a neural system, which shows a powerful modeling ability in various fields such as time-series forecasting (Chang and Chang, 2006), and evaporation estimation (Kisi, 2009). The architecture of the ANFIS consists of five layers, shown in Fig. 1, and their main features are briefly described as follows.

– *Layer 1 (input nodes):* each node of this layer generates membership grades that belong to each of the appropriate fuzzy sets by using membership functions. The Gaussian membership function becomes popular when identifying fuzzy sets owing to its smoothness and concise notations.

HESSD
10, 6153–6192, 2013

- *Layer 2 (rule node):* in this layer, either the AND operator is used to generate an output that represents the result of the antecedent for the rule, such as the firing strength.
- *Layer 3 (average nodes):* this layer is to normalize the results of the previous layer, which means to calculate the ratio of each *i*th rule's firing strength to the sum of all rules' firing strengths.
- *Layer 4 (consequent nodes):* the fourth layer is to compute the contribution of the each *i*th rule toward the total output.
- *Layer 5 (output nodes):* in this layer, every node computes the overall output by summing up all the incoming signals. And the defuzzification process transforms each rule's fuzzy results into a crisp output which is the desired real value in this layer.

The ANFIS is trained by a hybrid supervised learning algorithm, a gradient descent method and a least-squares method to optimize both linear and nonlinear parameters. Furthermore, it is critical to define the fuzzy rules when designing an ANFIS model because the number of parameters may increase enormously as the number of rules increases. A solution to this problem is to use the subtractive fuzzy clustering algorithm, which is devoted to minimizing the number of rules to effectively discriminate the fuzzy quality associated with each cluster. Details of the ANFIS algorithm coupled with the subtractive fuzzy clustering algorithm can be found in Chang and Chang (2006).

2.2 Landsat data

The Landsat Program is a series of Earth-observing satellite missions jointly managed by the National Aeronautics and Space Administration (NASA), the National Oceanic and Atmospheric Administration (NOAA) and the US Geological Survey (USGS). It provides the world with unprecedented information on land cover changes since 1972. The knowledge gained from four decades of continuous data contributes to research on

HESSD
10, 6153–6192, 2013

various aspects of the Earth and to evaluation of the dynamic changes caused by both natural processes and human practices. Landsat data and related researches have led to the improvement of human welfares, biodiversity health, energy and water management, urban planning, disaster recovery and agriculture monitoring. In this study, we use the data sets obtained from Landsat 5 and Landsat 7 for evaporation estimation over Taiwan Island. The images obtained from Landsat 5 are of multi-spectrum with seven bands consisting of VIS (visible region), NIR (near infrared) and TIR (thermal infrared) while the images obtained from Landsat 7 have eight bands consisting of VIS, NIR, TIR and SWIR (short wave infrared).

2.2.1 Enhanced vegetation index (EVI)

Vegetation indices measure the radiometric intensity of the amount, structure and condition on vegetation through spectral transformation of two or more bands obtained from satellites. The indices are used mainly to amplify vegetation signals and conduct both spatial and temporal comparisons of terrestrial photosynthetic activities and canopy variations. EVI is an optimized index designed to brighten vegetation signals with improved sensitivity in high biomass regions and vegetation monitoring by eliminating background and atmospheric noises (Huete et al., 1999). EVI is expressed as follows:

$$\mathrm{EVI} = G \times \frac{\rho_{\mathrm{NIR}} - \rho_{\mathrm{red}}}{(\rho_{\mathrm{NIR}} + C1 \times \rho_{\mathrm{red}} - C2 \times \rho_{\mathrm{blue}} + L)} \quad (1)$$

where ρ is the surface reflectance in the wavelength band; L is the canopy background adjustment that addresses non-linear, differential NIR and red radiant transfer through a canopy; and $C1$ and $C2$ are the coefficients to minimize the aerosol variations. In general, $L = 1$, $C1 = 6$, $C2 = 7.5$, and G (gain factor) = 2.5 (Huete et al., 2002; Karnieli and Dall'Olmo, 2003). EVI ranges from 0 (no vegetation) to nearly 1 (densest vegetation) and is sensitive to canopy structural variations, including the leaf area index, canopy type, plantphysiognomy and canopy architecture.

HESSD
10, 6153–6192, 2013

Staring from 2000, EVI was adopted as a standard product by NASA and became extremely popular owing to its capability of eliminating background and atmospheric noises and analyzing the greenness of vegetation that has a high correlation to evapotranspiration. Nagler et al. (2005) used EVI obtained from remotely sensed imagery and in-situ measurements to estimate evapotranspiration with respect to riparian vegetation along rivers and individual plant types. In this study, EVI was quantitatively evaluated using data of Landsat Enhanced Thematic Mapper Plus (ETM+) over Taiwan during 2001 and 2010.

2.2.2 Land surface temperature (LST)

LST is retrieved from Landsat Enhanced Thematic Mapper (ETM+) and Thematic Mapper (TM) images. Calculating LST from Landsat images involves a suite of steps: data correction of geometric distortions; data correction of radiometric distortions; conversion of digital numbers to radiance; calculation of the temperature in Kelvin; and conversion of the Kelvin to degrees Celsius (Li et al., 2004; Rhinane et al., 2012). In brief, Landsat images are first converted from digital numbers to radiance, and then to land surface temperature. The main conversion formulas are given by Landsat handbook (USGS, 1979):

$$L = \text{Bias} + (\text{Gain} \cdot \text{DN}) \tag{2}$$

where L is spectral radiance in $\text{W m}^{-2}\,\text{ster}^{-1}\,\mu\text{m}^{-1}$; Bias is the spectral radiance of the sensor for a DN of zero; Gain is the gradient of calibration; and DN is the digital number value recorded.

$$T = \frac{K_2}{\ln(K_1/L + 1)} \tag{3}$$

where T is the effectiveness at-satellite temperature in Kelvin; K_1 is calibration constant 1 (Table 1); K_2 is calibration constant 2 (Table 1); and L is spectral radiance

HESSD
10, 6153–6192, 2013

in $W m^{-2} ster^{-1} \mu m^{-1}$. Nemani and Running (1989) indicated infrared surface temperatures obtained from satellite sensors could be used to infer evaporation over large area. Therefore this study also adopted LST as another input to the proposed model.

2.2.3 Pre-processing of remote sensing data

The primary image data obtained from Landsat satellite are the WGS84 ellipsoid employed as the Earth model for the Universal Transverse Mercator (UTM). Without a comprehensive pre-process rectifying the separate estimation components of evaporation, it would be too difficult to properly quantify estimation errors. Therefore, primary image data are pre-processed in two stages: first being converted to radiance; and next being converted to reflectance. NASA provides many imagery product options of image conversion for Landsat satellites. This study uses Level 1G Product for both radiometrical and geometrical correction. For data converted from radiance to reflectance, this study uses the image processing software ENVI (Environment for Visualizing Images) to rectify Landsat images. The reflectance after conversion is affected by atmosphere, scattering or aerosols, which still causes a big noise. Therefore images require atmospheric corrections to reduce the impacts of water vapor, oxygen, carbon dioxide, methane and ozone on images. This study uses the ACRON (Atmosphere CORrection Now) software for atmospheric corrections. Figure 2 shows the reflectance results of vegetation before and after atmospheric corrections made by the ACRON, where obvious differences occur before and after atmospheric corrections.

3 Application

The continuous monitoring of regional evaporation from land surfaces is important for applications requiring spatial estimates of evaporation over large areas. There is a need to establish estimation models across the whole Taiwan. However the network of meteorological gauging stations is not dense enough in Taiwan. Remote sensing data could

HESSD
10, 6153–6192, 2013

be suitable to mitigate such shortcoming (Cleugh et al., 2007). This study intends to construct a regional evaporation estimation model primarily driven by solely remote sensing data across the whole Taiwan. In addition, an evaporation map across the whole Taiwan covering gauged and ungauged areas can be drawn.

3.1 Study area

Taiwan is an island country situated within the subtropical monsoon zone in East Asia of northern Pacific Ocean, where 32 % of the island is covered with rugged mountains, 31 % with hills and tablelands, and 37 % with plains. Evaporation differs from area to area in Taiwan because of the distinct variations in topographical and climatic conditions. This study adopts remote sensing data derived from satellite images of Landsat 5 and Landsat 7. Table 2 shows the statistics of the meteorological data collected at 16 meteorological gauging stations (Fig. 3), in which the correlation of meteorological variables with evaporation are in general not high enough, and therefore the meteorological data are regarded as ancillary data and will not be used for model construction in this study.

3.2 Data collection

3.2.1 Remote sensing data: for model construction

Landsat satellites pass over Taiwan at about 10 a.m. LT. In this study Landsat imagery used as primary data for measuring and detecting evaporation was provided at a span of 16 days from February 2001 to November 2010 by Landsat 5 and Landsat 7, which were equipped with Thematic Mapper (TM) and Enhanced Thematic Mapper (ETM+) sensors, respectively. A total of 342 images were collected. Nonetheless, Landsat imagery is limited to the low number of cloud-free scenes over humid climatic zones (Potter et al., 2007). With a revisiting schedule of 16 days for Landsat satellites, collecting

HESSD
10, 6153–6192, 2013

monthly cloud-free Landsat images is of low probability in our cases. Therefore, only 45 out of 342 images over the 10 yr investigation period could be used in this study.

Enhanced Vegetation Index (EVI; bands 1, 3 and 4)

In this study, EVI data are different from area to area due to vegetation and climatic conditions of the study areas. Table 3 shows the basic statistics of EVI at 16 gauging stations. A "0" EVI value indicates no vegetation, while a "nearly 1" EVI value indicates densest vegetation. In general, the more urbanized the cities are (such as Taipei and Banqiao), the smaller the EVI values are. However the EVI value of Kaohsiung City is comparatively high, which might be due to its low population density. Nagler (2005) proposed that the correlations between evapotranspiration and EVI were strong, and eight out of nine tower sites had correlation coefficients higher than 0.8. In this study, the correlations between EVI and evaporation are smaller than 0.7, which might be ascribed to the very different study area from that of Nagler (2005), and the dissimilar types of vegetation as well as the low image resolution (1 km × 1 km) of our study area.

Land Surface Temperature (LST; band 6)

LST data of Taiwan during 2001 and 2010 were derived from the imagery released by remote sensors operating in the thermal infrared wavelength of Landsat Thematic Mapper (TM) and Enhanced Thematic Mapper (ETM+). Figure 4 shows the comparison results between LST obtained from satellite imagery and thermometer temperatures obtained at meteorological gauging stations. The results indicate LST are higher than thermometer temperatures at 9 out of 16 stations. These nine stations are mainly located near coastal areas. The R^2 between LST and thermometer temperature is 0.75 (Fig. 5).

The impact of urbanization on LST in cities of this study area is observed (Table 3). LST is relatively high in cities, and clouds cause certain impacts on LST. LST at areas shaded by clouds is very low due to the prevention of the shaded areas from direct

HESSD
10, 6153–6192, 2013

sunlight. In addition, 12 out of 16 correlation coefficients between LST and evaporation are higher than 0.5, where 8 of them are higher than 0.6. It implies LST and evaporation are related in certain degrees. The average correlation coefficient between LST and evaporation is 0.58 (Table 3). Therefore, it is suitable to use LST as an input to the ANFIS model for evaporation estimation.

3.2.2 Meteorological data: for ancillary purpose

In this study, meteorological data were collected at 16 meteorological gauging stations distributed uniformly all over Taiwan from February 2001 to November 2010. The data collection period was the same as that of remote sensing data for ancillary purpose. Meteorological data collected in this study consist of seven types: evaporation (E: mm day^{-1}); wind speed (W: m s^{-1}); temperature (T: °C); humidity (H: %); sunshine hours (S: h day^{-1}); radiation (R: MJ m^{-2} day^{-1}) and dew point (D: °C) (Table 2). The locations of 16 meteorological gauging stations are illustrated in Fig. 3. Among the meteorological data collected, evaporation is the only variable selected to train the structure and test the performance for the ANFIS, while the other six meteorological variables are used only for characteristic analyses and are irrelevant to the construction of the ANFIS models.

3.3 Model construction

The network of meteorological gauging stations is not dense enough to provide sufficient data, which hinders the reliable estimation of evaporation for the whole Taiwan. The availability of remote sensing data, instead of ground measurements, shows good potential in evaporation estimation. In addition, the ANFIS inherits powerful ability from a combination of fuzzy logics and artificial neural techniques in dealing with the uncertainty and imprecision of systems. The proposed ANFIS model with inputs based solely on remote sensing data underpins the modeling approach, in particular under the circumstances with limited data.

HESSD
10, 6153–6192, 2013

To investigate the reliability and applicability of the constructed ANFIS models, two types (i.e. temporal and spatial) models are configured and tested. The models are driven with the same ten-year data of EVI and LST derived from Landsat images. The first type (Model-T) is configured by temporal input allocation: data retrieved from the first half (2001–2003), the subsequent three-tenth (2004–2005) and the last one-fifth (2006–2010) data collection periods are allocated into the training, validation and testing datasets of the ANFIS accordingly. Model-T intends to incorporate data covering all 16 meteorological gauging stations into each processing stages of the ANFIS so that provide clear temporal characteristics of evaporation for the whole Taiwan. The second type (Model-S) is configured by spatial input allocation: data retrieved from nine, three and four meteorological gauging stations are allocated into training, validation and testing datasets of the ANFIS accordingly. The distinct station-based data arranged into a processing phases implies Model-S can be appropriate for estimating evaporation at ungauged sites (the stations used in the testing phase are assumed as ungauged sites). The data allocation of Models-T and -S for the ANFIS is illustrated in Table 4. For each model, two input combinations are evaluated: a composite of the EVI and LST; and LST only.

In this study, the radius of the ANFIS that defines the neighborhood of a cluster center is determined through the subtractive fuzzy clustering, and the radius ranges from 0.05 to 0.95. Fuzzy rules can be determined automatically as the radius is fixed.

Assessment of model performance

Model performance of different input combinations is evaluated based on the criteria of the root mean square error (RMSE), mean absolute error (MAE), coefficient of efficiency (CE), and correlation coefficient (CC). RMSE and MAE are quantitative measures for illustrating the predictive capability of a model. CE measures the degree to which the model predictions match the observations. CC is a frequently used index for assessing the correlation between two variables. The formulas are given as follows:

HESSD
10, 6153–6192, 2013

$$\mathrm{RMSE} = \sqrt{\frac{\sum_{i=1}^{n}[o_i - e_i]^2}{n}} \tag{4}$$

$$\mathrm{MAE} = \frac{\sum_{i=1}^{n}|o_i - e_i|}{n} \tag{5}$$

$$\mathrm{CE} = 1 - \frac{\sum_{i=1}^{n}(o_i - e_i)^2}{\sum_{i=1}^{n}(o_i - \overline{o})^2} \tag{6}$$

$$\mathrm{CC} = \frac{\sum_{i=1}^{n}\left(o_i - \overline{o}\right)\left(e_i - \overline{e}\right)}{\sqrt{\sum_{i=1}^{n}\left(o_i - \overline{o}\right)^2 \sum_{i=1}^{n}\left(e_i - \overline{e}\right)^2}} \tag{7}$$

where o_i, $\overline{o}$, e_i and $\overline{e}$ are the observed values, average of observed values, predicted values and average of predicted values, respectively, and n is the number of data.

This study also adopts Skill Score (SS) as an index to distinguish the performance of two models.

$$\mathrm{SS} = \frac{(E_{\mathrm{RM}} - E_{\mathrm{TM}})}{E_{\mathrm{RM}}} \times 100\% \tag{8}$$

where E_{RM} is the error of the reference model, and E_{TM} is the error of the target (our) model. SS measures forecast accuracy relative to the reference forecast.

HESSD
10, 6153–6192, 2013

3.4 Derivation of evaporation maps across Taiwan

In this study, five sub-regional evaporation maps derived from five Landsat imagery were seamed together to yield one evaporation map across Taiwan. The ideal condition would be all five images were collected on the same date. However the five Landsat images for use were obtained on different dates due to various cloud conditions in the region and image quality concerns, therefore the derived evaporation map represents a short period (within a month) rather than one single day. Figure 6 shows an example of five sub-Landsat images relevant to the whole Taiwan. The original pixel resolution of Landsat imagery is 30 m × 30 m. The resolution is too high to use due to great time-consuming computation process for evaporation estimation. Therefore, the Landsat imagery was resized into 1 km × 1 km by the nearest neighborhood method.

4 Results and discussion

The regional evaporation estimation through a neuro-fuzzy network driven by remotely sensed data was achieved in this study. Previous researches that used remote sensing techniques to estimate evaporation over large areas were mainly devoted to continental climates, whose hydrology, geomorphology and vegetation types are not as complex and diverse as those in this study. The vegetation types of this study area are very different from area to area. Using EVI as an input to the ANFIS for evaporation estimation is another approach because EVI can reflect the overall vegetation condition and thus might help increase estimation accuracy. Table 5 shows the CC values between EVI and six meteorological factors, where the top two highest correlation coefficients (+, −) at individual meteorological gauging stations are marked in bold and underlined, respectively. The largest CC value (0.89) is not high enough, which indicates that the EVI of the study area is very complex and thus is not easy to be incorporated with other meteorological factors for evaporation estimation. Table 5 also reveals thermometer temperature, radiation and dew point are the most relevant meteorological factors to

HESSD
10, 6153–6192, 2013

EVI, which may imply EVI contains information about radiation and dew point. In addition EVI and radiation are highly correlated in cities such as Taipei and Banqiao. The same practice applied to cities is more acceptable because temperature variation in cities is not as violent as that in mountains or other sites. In brief, EVI obtained from Landsat imagery should have certain relationship with meteorological phenomena in Taiwan.

Table 6 shows the best ANFIS structure (in bold) for each model identified by the RMSE in the testing phases. For Model-T with inputs EVI and LST, the structure with the radius (r_a) = 0.30 and 6 rules is identified the best owing to the smallest RMSE value. For Model-T with LST as the only input, the structure with r_a = 0.35 and 5 rules is identified the best. Similarly, the best ANFIS structures for Model-S are successfully identified.

4.1 Analysis of model performance

The inputs dimension of the ANFIS is four, which are EVI (band 1, band 3 and band 4) and LST (band 6) retrieved from Landsat remote sensing data. Model-T (temporal input allocation) aims to give good evidence to characterize evaporation for the whole Taiwan on the basis of data covering 16 gauging stations in each processing phases of the ANFIS. Alternatively, Model-S (spatial input allocation) aims to estimate evaporation at ungauged sites (12 gauge stations and 4 assumed ungauged sites). This approach is essential when creating an evaporation map across Taiwan, where meteorological gauging stations are not set up anywhere or anytime all over this island.

The estimation results of Model-T shown in Figs. 7a and 8a reveal that the trend of estimations keeps close to observations except at extreme values, which implies EVI and LST are not the only factors that affect evaporation. Therefore, EVI and LST can be used to properly estimate evaporation through Model-T, except at the extreme values. Figures 7 and 8 also point out Model-T is superior to Model-S, however, Model-S still catches the evaporation trend.

HESSD
10, 6153–6192, 2013

Figure 9a shows that Model-T with training data corresponding to all 16 meteorological gauging stations can estimate more accurately than Model-S, in terms of small MAE and RMSE, and higher CE and CC. The results manifest that Model-T is more appropriate for characterizing the evaporation for all the meteorological gauging stations owing to sufficient training data from all 16 gauging stations. The clues revealed from Table 3 indicate evaporation has its own pattern at every meteorological gauging station, which also account for the superiority of Model-T over Model-S.

Figure 9b illustrates the comparison results of SS for Models-T and -S with different input combinations. In brief, models with two inputs (EVI and LST) can perform more accurately, as expected, than those with only one input (LST), which also demonstrates Model-T is superior to Model-S in testing phases. It suggests Model-T (temporal input allocation) is suitable for making island-wide evaporation estimation while Model-S (spatial input allocation) is suitable for making evaporation estimation at ungauged sites.

In addition, the results summarized in Fig. 9 show that the models with two inputs (EVI and LST) can estimate more accurately than those with only one input (LST), which demonstrates EVI indeed benefits the estimation process but with less improvement. In practice, EVI requires atmospheric corrections, which is a complex and time-consuming process. Nevertheless, LST obtained from remote sensing data does not require atmospheric corrections. It would be more convenient and economical to conduct evaporation estimation just based on LST if its error tolerance is acceptable.

4.2 Assessment on evaporation maps

Figure 10 shows the evaporation maps obtained from Models-T and -S with different input combinations. The maps indicate the models with only one input shown in Fig. 10a.2 and 10b.2 can be used to estimate evaporation, which is similar to the model with two inputs shown in Fig. 10a.1 and 10b.1. However the impact of clouds on Fig. 10a.2 and 10b.2 is more obvious than that of Fig. 10a.1 and 10b.1, which may be attributed to the higher sensitivity of LST to clouds. In brief, Model-T (EVI, LST)

HESSD
10, 6153–6192, 2013

produces higher estimation values than Model-S (EVI, LST) in cities; models with only one input (LST) are more sensitive to clouds and produce higher estimation values of evaporation in cities; and Model-S (LST) produces higher estimation values than Model-T (LST) in cities. Even though EVI contributes to evaporation estimation, the model with only one input (LST) can suitably capture the evaporation trend and perform well if Landsat imagery is interspersed with few clouds (Fig. 10).

Consequently, an island-wide evaporation map across Taiwan can be successfully produced by seaming five sub-regional evaporation maps (northwest, northeast, middle-west, middle-east, south regions) derived from Landsat imagery. Figure 11 displays the evaporation maps across Taiwan obtained from Models -T and -S with two inputs, respectively. Evidence shows Model-S in general produces higher estimation values than Model-T, which suggests models with spatial input allocation produce higher evaporation values than models with temporal input allocation.

5 Conclusions

This study aimed to construct an effective evaporation estimation model that possesses the ability to present the spatial distribution of evaporation across Taiwan through a neural fuzzy network based solely on Landsat remote sensing data (EVI, LST), without ground-based meteorological data. The retrieval of the EVI and LST was conducted through a series of data preprocessing steps facilitated by relevant Landsat products. The results indicate that the proposed ANFIS model can effectively produce the spatial variation of evaporation estimations and accurately capture the evaporation trend with acceptable errors of about 1 mm day^{-1}.

The study area covered 16 meteorological gauging stations whose characteristics such as vegetation types, climate conditions and elevations are different from place to place. It is obvious different areas have their own EVI patterns. The aforementioned phenomena could result in low correlations between evaporation and meteorological variables. Nevertheless, the correlation between LST and thermometer temperature

HESSD
10, 6153–6192, 2013

are quite high, and therefore LST was adopted as a model input for estimating evaporation. Therefore, two types of input combinations to the estimation model were investigated: (1) EVI and LST; and (2) LST. The results indicate models fed only with LST well capture evaporation trend and produce adequate evaporation estimation. Models fed with EVI and LST can make better evaporation estimation than those fed only with LST. It is noticed clouds in Landsat imagery will lead to lower LST and thus result in an underestimation of evaporation. The study also shows that EVI can improve the estimation accuracy; however, large bias may occur in the vicinity of peak values. The results suggests Model-T (temporal input allocation) is suitable for making island-wide evaporation estimation while Model-S (spatial input allocation) is suitable for making evaporation estimation at ungauged sites. In summary, the results suggest the proposed models incorporated with remote sensing data for evaporation estimation are reliable and applicable over large areas where the network of ground-based meteorological gauging stations is not dense enough or readily available.

Acknowledgements. This study was funded by the National Science Council, Taiwan, ROC (Grant number: 100-2313-B-002-011-MY3). The Landsat data and meteorological gauge data provided by the Central Weather Bureau, Taiwan, ROC, are very much appreciated.

References

Abrahart, R. J., Anctil, F., Coulibaly, P., Dawson, C. W., Mount, N. J., See, L. M., Shamseldin, A. Y., Solomatine, D. P., Toth, E., and Wilby, R. L.: Two decades of anarchy? Emerging themes and outstanding challenges for neural network river forecasting, Prog. Phys. Geogr., 36, 480–513, 2012.

Anderson, M. C., Kustas, W. P., Norman, J. M., Hain, C. R., Mecikalski, J. R., Schultz, L., González-Dugo, M. P., Cammalleri, C., d'Urso, G., Pimstein, A., and Gao, F.: Mapping daily evapotranspiration at field to continental scales using geostationary and polar orbiting satellite imagery, Hydrol. Earth Syst. Sci., 15, 223–239, doi:10.5194/hess-15-223-2011, 2011.

HESSD

10, 6153–6192, 2013

Bateni, S. M., Entekhabi, D., and Castelli, F.: Mapping evaporation and estimation of surface control of evaporation using remotely sensed land surface temperature from a constellation of satellites, Water Resour. Res., 49, 950–968, doi:10.1002/wrcr.20071, 2013.
Blyth, E. and Harding, R. J.: Methods to separate observed global evapotranspiration into the interception, transpiration and soil surface evaporation components, Hydrol. Process., 25, 4063–4068, 2011.
Cammalleri, C., Anderson, M. C., Ciraolo, G., D'Urso, G., Kustas, W. P., La Loggia, G., and Minacapilli, M.: The impact of in-canopy wind profile formulations on heat flux estimation in an open orchard using the remote sensing-based two-source model, Hydrol. Earth Syst. Sci., 14, 2643–2659, doi:10.5194/hess-14-2643-2010, 2010.
Chang, F. J. and Chang, Y. T.: Adaptive neuro-fuzzy inference system for prediction of water level in reservoir, Adv. Water Res., 29, 1–10, 2006.
Chang, F. J., Chang, L. C., Kao, H. S., and Wu, G. R.: Assessing the effort of meteorological variables for evaporation estimation by self-organizing map neural network, J. Hydrol., 384, 118–129, 2010.
Chang, F. J., Sun, W., and Chung, C. H.: Dynamic factor analysis and artificial neural network for estimating pan evaporations at multiple stations in northern Taiwan, Hydrolog. Sci. J., 58, 813–825, doi:10.1080/02626667.2013.775447, 2013.
Chen, Y. H. and Chang, F. J.: Evolutionary artificial neural networks for hydrological systems forecasting, J. Hydrol., 367, 125–137, 2009.
Chiang, Y. M. and Chang, F. J.: Integrating hydrometeorological information for rainfall-runoff modelling by artificial neural networks, Hydrol. Process., 23, 1650–1659, 2009.
Chung, C.-H., Chiang, Y.-M., and Chang, F.-J.: A spatial neural fuzzy network for estimating pan evaporation at ungauged sites, Hydrol. Earth Syst. Sci., 16, 255–266, doi:10.5194/hess-16-255-2012, 2012.
Cleugh, H. A., Leuning, R., Mu, Q., and Running, S. W.: Regional evaporation estimates from flux tower and MODIS satellite data, Remote Sens. Environ., 106, 285–304, 2007.
Contreras, S., Jobbágy, E. G., Villagra, P. E., Nosetto, M. D., and Puigdefábregas, J.: Remote sensing estimates of supplementary water consumption by arid ecosystems of central Argentina, J. Hydrol., 397, 10–22, 2011.
Coulomb, C. V., Legessea, D., Gassea, F., Travic, Y., and Chernetd, T.: Lake evaporation estimates in tropical Africa (Lake Ziway, Ethiopia), Hydrol. Process., 245, 1–18, 2001.

HESSD
10, 6153–6192, 2013

Cristóbal, J., Poyatos, R., Ninyerola, M., Llorens, P., and Pons, X.: Combining remote sensing and GIS climate modelling to estimate daily forest evapotranspiration in a Mediterranean mountain area, Hydrol. Earth Syst. Sci., 15, 1563–1575, doi:10.5194/hess-15-1563-2011, 2011.

Donohue, R. J., McVicar, T. R., and Roderick, M. L.: Assessing the ability of potential evaporation formulations to capture the dynamics in evaporative demand within a changing climate, J. Hydrol., 386, 186–197, 2010.

Farah, H. O. and Bastiaanssen, W. G. M.: Impact of spatial variations of land surface parameters on regional evaporation: a case study with remote sensing data, Hydrol. Process., 15, 1585–1607, 2011.

Glenn, E. P., Doody, T. M., Guerschman, J. P., Huete, A. R., King, E. A., McVicar, T. R., Van Dijk, A. I. J. M., Van Niel, T. G., Yebra, M., and Zhang, Y.: Actual evapotranspiration estimation by ground and remote sensing methods: the Australian experience, Hydrol. Process., 25, 4103–4116, 2011.

Huete, A., Justice, C., and Van Leeuwen, J. D.: MODIS Vegetation Index (Mod 13) Algorithm Theoretical Basis Document Version 3, University of Arizona, Tucson, USA, 1999.

Huete, A., Didan, K., Miura, T., Rodriguez, E. P., Gao, X., and Ferreira, L. G.: Overview of the radiometric and biophysical performance of the MODIS vegetation indices, Remote Sens. Environ., 83, 195–213, 2002.

Jang, J. S. R.: ANFIS-adaptive-network-based fuzzy inference system, IEEE T. Syst. Man. Cyb., 23, 665–685, 1993.

Jiang, L. and Islam, S.: Estimation of surface evaporation map over southern Great Plains using remote sensing data, Water Resour. Res., 37, 329–340, 2001.

Karnieli, A. and Dall'Olmo, G.: Remote-sensing monitoring of desertification, phenology, and droughts, Manage. Environ. Qual., 14, 22–38, 2003.

Kim, S. and Kim, H. S.: Neural networks and genetic algorithm approach for nonlinear evaporation and evapotranspiration modeling, J. Hydrol., 351, 299–317, 2008.

Kisi, O.: Daily pan evaporation modeling using multi-layer perceptrons and radial basis neural network, Hydrol. Process., 23, 213–223, 2009.

Landeras, G., Ortiz-Barredo, A., and Lopez, J. J.: Comparison of artificial neural network models and empirical and semi-empirical equations for daily reference evapotranspiration estimation in the Basque country (Northern Spain), Agr. Water Manage., 95, 553–565, 2008.

HESSD
10, 6153–6192, 2013

Li, F., Jackson, T. J., Kustas, W. P., Schmugge, T. J., French, A. N., Cosh, M. H., and Bindlish, R.: Deriving land surface temperature from Landsat 5 and 7 during SMEX02/SMACEX, Remote Sens. Environ., 92, 521–534, 2004.

Liu, S., Mo, X., Zhao, W., Naeimi, V., Dai, D., Shu, C., and Mao, L.: Temporal variation of soil moisture over the Wuding River basin assessed with an eco-hydrological model, in-situ observations and remote sensing, Hydrol. Earth Syst. Sci., 13, 1375–1398, doi:10.5194/hess-13-1375-2009, 2009.

Matsushita, B. and Fukushima, T.: Methods for retrieving hydrologically significant surface parameters from remote sensing: a review for applications to east Asia region, Hydrol. Process., 23, 524–533, 2009.

Nagler, P. L.: Evapotranspiration on western US rivers estimated using the Enhanced Vegetation Index from MODIS and data from eddy covariance and Bowen ratio flux towers, Remote Sens. Environ., 97, 337–351, 2005.

Nemani, R. and Running, S. W.: Estimation of regional surface resistance to evapotranspiration from NDVI and thermal IR AVHRR data, J. Appl. Meteorol., 28, 276–284, 1989.

Parasuraman, K., Elshorbagy, A., and Carey, S. K.: Modelling the dynamics of the evapotranspiration process using genetic programming, Hydrolog. Sci. J., 52, 563–578, 2007.

Potter, C., Gross, P., Genovese, V., and Smith, M. L.: Net primary productivity of forest stands in New Hampshire estimated from Landsat and MODIS satellite data, Carbon Balance Manag., 2, 1–11, doi:10.1186/1750-0680-2-9, 2007.

Rhinane, H., Hilali, A., Bahi, H., and Berrada, A.: Contribution of Landsat TM Data for the Detection of Urban Heat Islands Areas Case of Casablanca, J. Geogr. Inf. Syst., 4, 20–26, 2012.

Rivas, R. and Caselles, V.: A simplified equation to estimate spatial reference evaporation from remote sensing-based surface temperature and local meteorological data, Remote Sens. Environ., 93, 68–76, 2004.

Shiri, J. and Kisi, O.: An application of artificial intelligence to estimate daily pan evaporation using available and estimated climatic data in the Khozestan Province (South West Iran), J. Irrig. Drain. D.-ASCE, 137, 412–425, 2011.

HESSD

10, 6153–6192, 2013

Sims, D. A., Rahman, A. F., Vicente, D., Cordova, V. D., El-Masri, B. Z., Baldocchi, D. D., Bolstad, P. V., Flanagan, L. B., Goldstein, A. H., Hollinger, D. Y., Misson, L., Monson, R. K., Oechel, W. C., Schmid, H. P., Wofsy, S. C., and Xu, L.: A new model of gross primary productivity for North American ecosystems based solely on the enhanced vegetation index and land surface temperature from MODIS, Remote Sens. Environ., 112, 1633–1646, 2008.

Sucksdorff, Y. and Ottle, C.: Application of satellite remote sensing to estimate areal evapotranspiration over a watershed, J. Hydrol., 121, 321–333, 1990.

Sudheer, K. P., Gosain, A. K., Rangan, D. M., and Saheb, S. M.: Modelling evaporation using an artificial neural network algorithm, Hydrol. Process., 16, 3189–3202, 2002.

US Geological Survey and the National Aeronautics and Space Administration: Landsat Data Users Handbook, 3rd Edn., Washington, USA, 1979.

Wang, W., Huang, D., Wang, X.-G., Liu, Y.-R., and Zhou, F.: Estimation of soil moisture using trapezoidal relationship between remotely sensed land surface temperature and vegetation index, Hydrol. Earth Syst. Sci., 15, 1699–1712, doi:10.5194/hess-15-1699-2011, 2011.

HESSD
10, 6153–6192, 2013

Table 1. ETM+ and TM Thermal Band Calibration Constants (from Landsat Handbook).

	K_1 (Constant 1) $W\,m^{-2}\,ster^{-1}\,\mu m^{-1}$	K_2 (Constant 2) K
Landsat 5	607.76	1260.56
Landsat 7	666.09	1282.71

HESSD
10, 6153–6192, 2013

Table 2. Statistics of meteorological gauging stations and meteorological variables.

Station	ELV.[1]	Evap.[2]	Temp.[3] (thermometer, °C)		Wind speed ($m s^{-1}$)		Humidity (%)		Sunshine hours (h)		Radiation ($MJ m^{-2} day^{-1}$)		Dew point (°C)	
	(m)	($mm day^{-1}$)	Mean	Mean	CC[4]	Mean	CC	Mean	CC	Mean	CC	Mean	CC	Mean	CC
Anbu	826	2.4	17.3	0.63	2.83	0.17	78.9	0.14	6.83	0.71	17.8	0.79	13.4	0.55
Banqiao	10	4.1	23.4	0.74	2.07	0.31	68.6	−0.52	8.76	0.42	16.0	0.59	17.0	0.61
Keelung	27	3.5	22.8	0.71	2.13	0.41	70.4	−0.46	7.90	0.69	12.8	0.83	16.9	0.42
Jutzhu	607	2.4	18.9	0.44	1.3	0.21	76.3	−0.35	7.21	−0.39	12.2	0.11	14.6	0.32
Yilan	7	2.7	22.1	0.53	1.98	0.49	74.3	0.17	8.61	0.45	15.3	0.72	17.1	0.51
Su-ao	25	4.9	22.6	0.59	2.73	0.19	75.3	−0.39	8.35	0.12	15.3	0.19	17.8	0.49
Hualien	16	3.0	22.8	0.51	2.89	0.27	73.4	−0.09	7.19	0.23	12.4	0.48	17.6	0.42
Sun Moon Lake	1015	3.0	19.2	0.5	1.32	0.31	73.8	0.07	8.13	0.28	15.9	0.62	14.1	0.38
Kaohsiung	2	4.0	25.1	0.62	1.93	0.00	71.5	0.19	9.43	0.47	16.4	0.64	19.4	0.54
Cheng-Kung	34	4.3	24.1	0.79	2.95	0.02	73.1	0.28	6.84	0.82	15.8	0.57	18.8	0.69
Alishan	2413	1.8	10.6	0.42	1.16	0.51	80.6	−0.36	6.84	0.57	17.1	0.63	6.9	0.12
Dawu	8	4.2	25.1	0.57	2.16	−0.14	70.9	0.00	7.36	0.60	15.0	0.49	19.2	0.40
Taipei	5	3.6	23.6	0.43	2.23	0.59	66.9	−0.48	8.87	0.27	14.7	0.74	16.8	0.26
Taichung	84	3.2	22.3	0.68	1.26	0.74	69.5	−0.20	8.80	0.00	13.4	0.63	16.0	0.58
Chiayi	27	3.7	23.3	0.71	1.76	0.43	75.9	−0.26	9.17	0.28	19.4	0.44	18.5	0.58
Taitung	9	4.2	24.8	0.78	1.81	0.05	68.7	0.35	7.53	0.70	18.8	0.79	18.5	0.71

[1]Elevation (m.a.s.l.).
[2]Evaporation.
[3]Temperature.
[4]Correlation with evaporation.

HESSD
10, 6153–6192, 2013

Table 3. Basic statistics of gauging stations, EVI and LST.

Station	EVI (Enhanced Vegetation Index) ∈ (0–1)			LST (Land surface temperature) (°C)		
	Mean	SD[1]	CC[2]	Mean	SD	CC
Anbu	0.50	0.06	0.35	18.2	3.53	0.55
Banqiao	0.37	0.11	0.65	25.2	4.32	0.87
Keelung	0.44	0.08	0.47	22.7	2.93	0.70
Jutzhu	0.47	0.07	0.05	19.3	2.97	0.32
Yilan	0.52	0.09	0.27	23.2	2.85	0.33
Su-ao	0.59	0.12	−0.32	22.2	2.47	0.23
Hualien	0.56	0.10	−0.02	22.2	3.45	0.56
Sun Moon Lake	0.49	0.09	−0.05	20.7	3.03	0.56
Kaohsiung	0.53	0.11	0.27	24.4	2.76	0.70
Cheng-Kung	0.56	0.09	0.19	23.2	3.14	0.70
Alishan	0.50	0.05	−0.27	15.7	3.66	0.46
Dawu	0.56	0.09	−0.15	22.4	3.55	0.57
Taipei	0.25	0.07	0.60	24.3	3.97	0.62
Taichung	0.41	0.09	0.58	23.5	3.48	0.70
Chiayi	0.52	0.10	0.43	24.5	3.62	0.63
Taitung	0.56	0.11	−0.24	22.7	3.17	0.70

[1] Standard deviation.
[2] Correlation with evaporation.

HESSD
10, 6153–6192, 2013

Table 4. Data allocation to the ANFIS for Model-T and Model-S.

Model	Training	Validation	Testing
Model-T Years	2001–2003	2004–2005	2006–2010
Model-S (Station)			
Anbu	◎		
Banqiao	◎		
Keelung	◎		
Jutzhu	◎		
Yilan	◎		
Su-ao	◎		
Hualien	◎		
Sun Moon Lake	◎		
Kaohsiung	◎		
Cheng-Kung		◎	
Alishan		◎	
Dawu		◎	
Taipei			◎
Taichung			◎
Chiayi			◎
Taitung			◎

HESSD
10, 6153–6192, 2013

Table 5. Correlation coefficients between EVI and meteorological factors.

Station	Temperature (thermometer, °C)	Wind speed ($m s^{-1}$)	Humidity (%)	Sunshine hours (h)	Radiation ($MJ m^{-2} day^{-1}$)	Dew point (°C)
Anbu	**0.74**	−0.08	0.36	0.00	0.46	0.72
Banqiao	0.42	0.34	−0.38	0.50	**0.89**	0.32
Keelung	0.52	0.07	0.05	0.43	**0.55**	0.51
Jutzhu	0.52	−0.01	0.42	0.07	0.37	**0.58**
Yilan	0.32	**0.62**	0.25	0.14	0.49	0.33
Su-ao	**−0.47**	−0.40	0.29	−0.19	−0.30	−0.40
Hualien	−0.06	**−0.22**	−0.04	0.03	0.15	−0.07
Sun Moon Lake	0.01	**−0.37**	−0.19	0.08	−0.20	−0.08
Kaohsiung	**0.43**	−0.21	0.13	−0.03	−0.07	0.37
Chiayi	0.67	−0.13	0.23	0.00	0.15	**0.69**
Cheng -Kung	**0.29**	−0.08	0.08	−0.01	−0.11	0.25
Alishan	0.08	**−0.28**	0.07	−0.10	−0.07	0.11
Dawu	−0.22	0.40	−0.16	−0.54	**−0.60**	−0.22
Taipei	0.32	0.50	−0.43	0.15	**0.67**	0.18
Taichung	**0.62**	0.22	−0.13	−0.60	0.25	0.53
Chiayi	0.67	−0.13	0.23	0.00	0.15	**0.69**
Taitung	−0.20	0.15	**−0.26**	−0.05	−0.11	−0.24
Subtotal*	8	5	7	4	7	7

* Numbers of the top two highest absolute CC valuesat each meteorological station: the highest correlation (in bold) and the second highest correlation (underlined).

HESSD
10, 6153–6192, 2013

Table 6. Model selection results of Model-T and Model-Swith respect to the ANFIS in the testing phases.

	Model-T				Model-S			
Inputs	EVI, LST		LST		EVI, LST		LST	
Radius (r_a)	Rules	RMSE	Rules	RMSE	Rules	RMSE	Rules	RMSE
0.05	166	9.9	166	7.0E+05	162	2.020	63	9.0E+03
0.10	79	2.E0+05	79	1.16	94	2.0E+02	16	1.235
0.15	33	4.07	33	1.06	32	16.11	8	1.236
0.20	18	1.65	18	1.09	16	1.52	6	1.198
0.25	9	1.16	9	1.05	9	1.26	3	1.193
0.30	**6**	**1.00**	6	1.05	7	1.19	3	1.192
0.35	5	1.08	**5**	**1.04**	**5**	**1.13**	3	1.190
0.40	3	1.01	3	1.05	5	1.14	3	1.190
0.45	2	1.04	2	1.05	5	1.16	**3**	**1.189**
0.50	2	1.05	2	1.05	3	1.14	1	1.202
0.55	1	1.05	1	1.05	2	1.20	1	1.202
0.60	1	1.05	1	1.05	1	1.18	1	1.202
0.95	1	1.05	1	1.05	1	1.180	1	1.202

Remark: the optimal models are marked in bold.

HESSD
10, 6153–6192, 2013

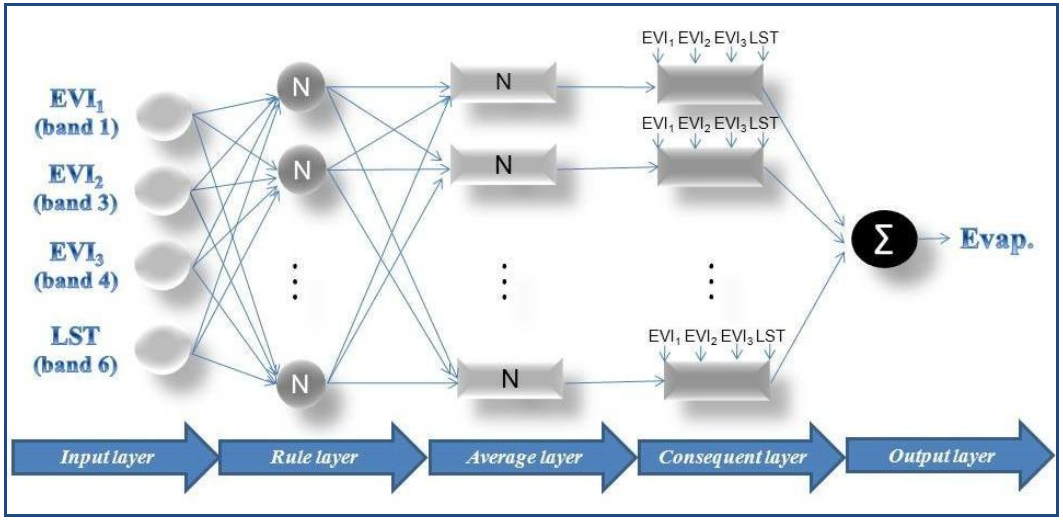

Fig. 1. ANFIS architecture in this study.

HESSD
10, 6153–6192, 2013

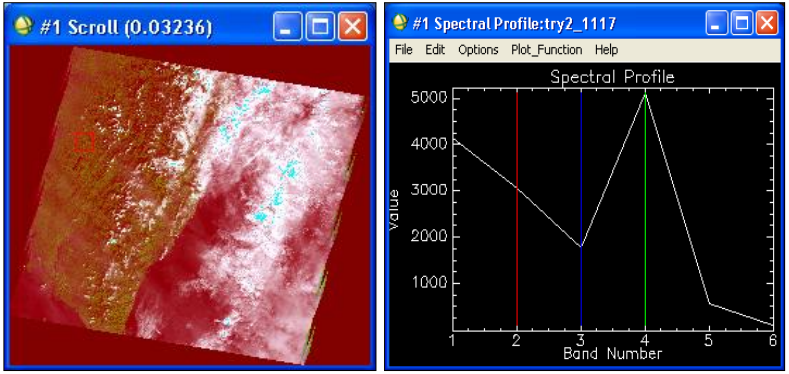

(a.1) image before correction (a.2) reflectance before correction

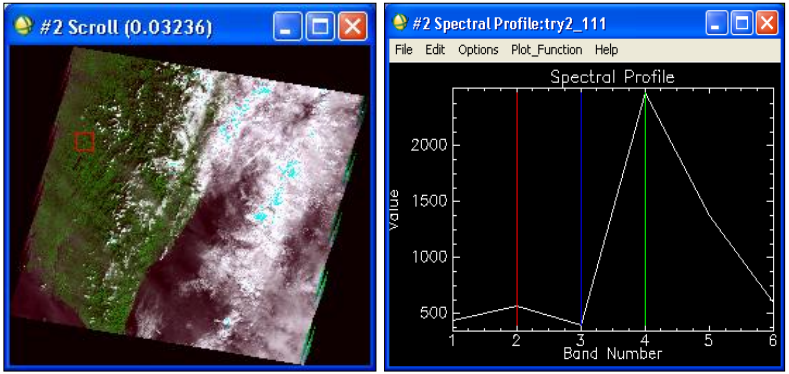

(b.1) image after correction (b.2) reflectance after correction

Fig. 2. Reflectance results of vegetation before and after atmospheric corrections made by the ACRON.

HESSD
10, 6153–6192, 2013

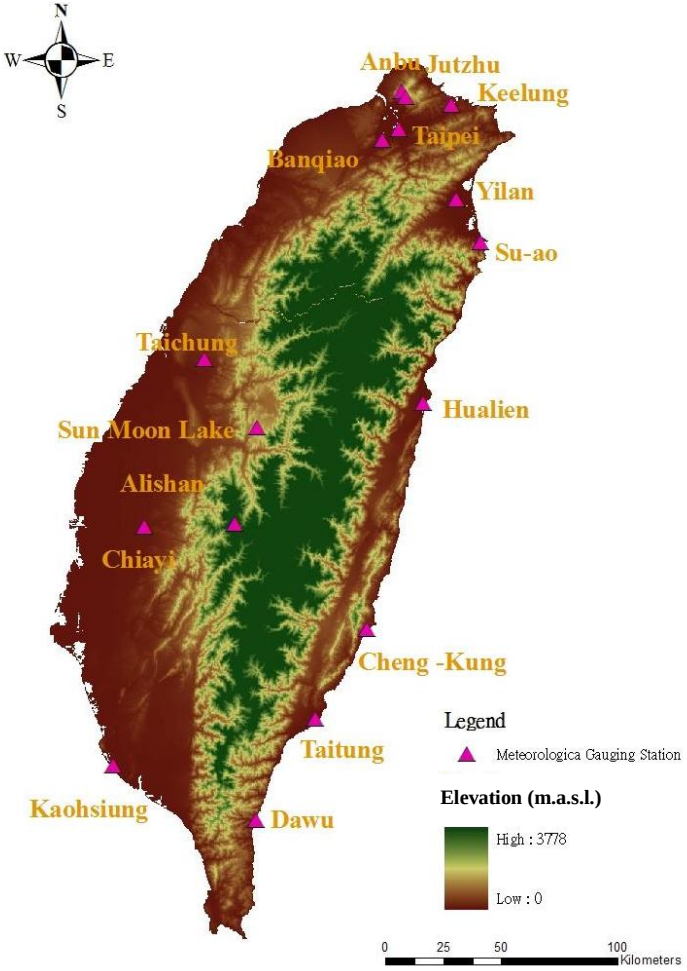

Fig. 3. Locations of meteorological gauging stations in Taiwan.

HESSD
10, 6153–6192, 2013

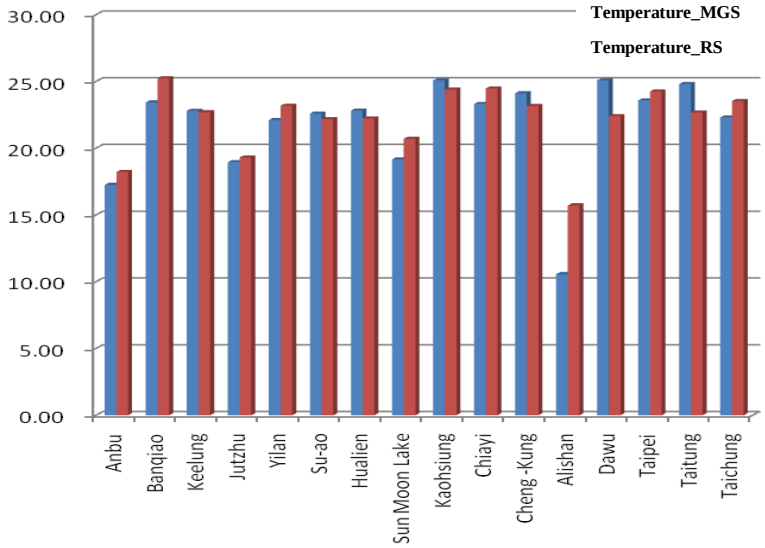

Fig. 4. Comparison of mean surface temperatures (LST vs. thermometer temperature).

HESSD
10, 6153–6192, 2013

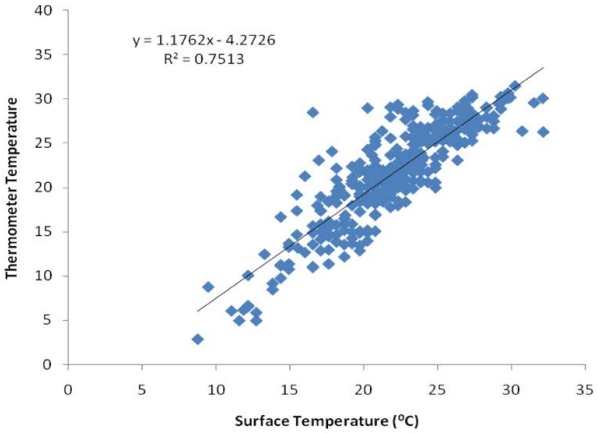

(a)

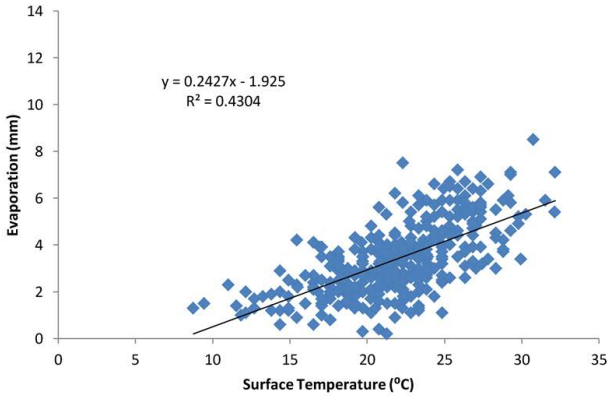

(b)

Fig. 5. Scatter plots of LST vs. **(a)** thermometer temperature; and **(b)** evaporation.

HESSD
10, 6153–6192, 2013

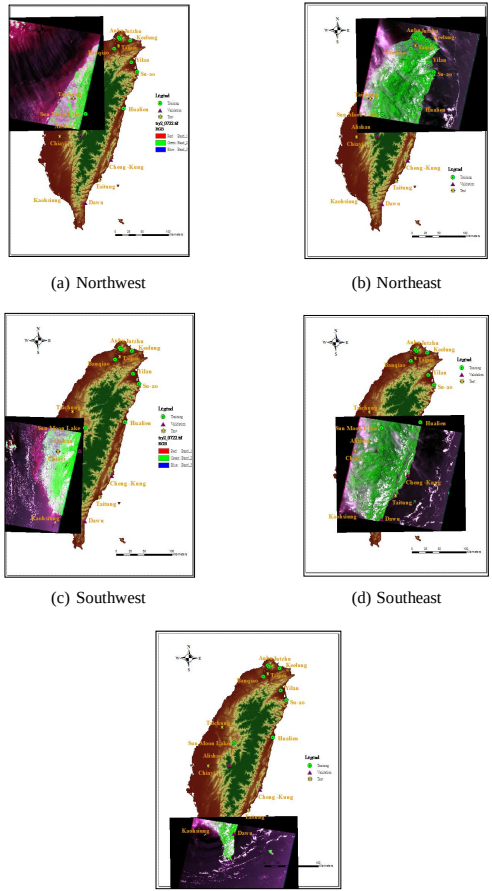

(a) Northwest (b) Northeast

(c) Southwest (d) Southeast

(e) Lower south

Fig. 6. Example of five sub-Landsat images relevant to the whole Taiwan.

HESSD
10, 6153–6192, 2013

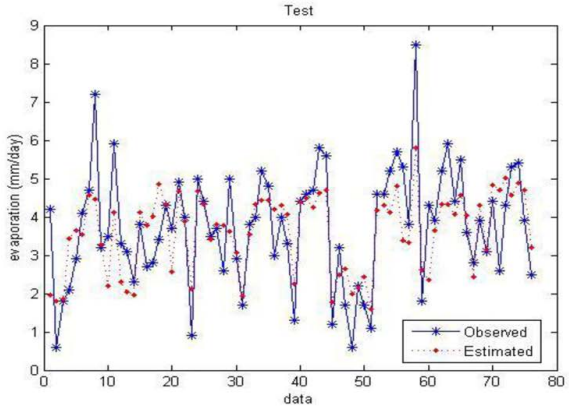

(a) Model-T (EVI, LST)

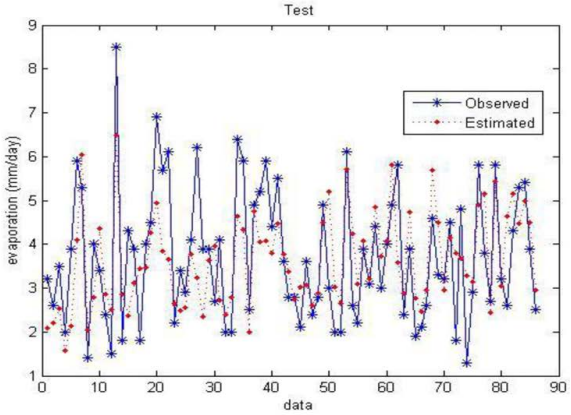

(b) Model-S (EVI, LST)

Fig. 7. Estimation performance of ANFIS models in the testing phases.

HESSD
10, 6153–6192, 2013

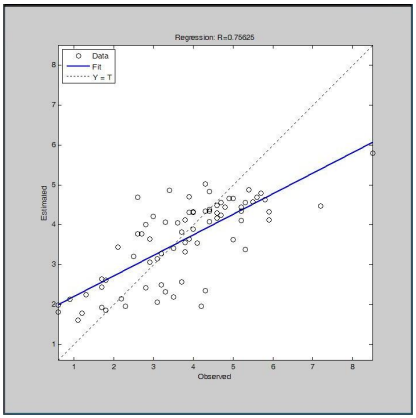

(a) Model-T (EVI, LST)

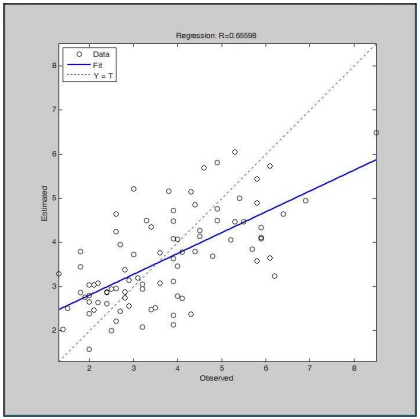

(b) Model-S (EVI, LST)

Fig. 8. Regression plots of ANFIS models in the testing phase.

HESSD
10, 6153–6192, 2013

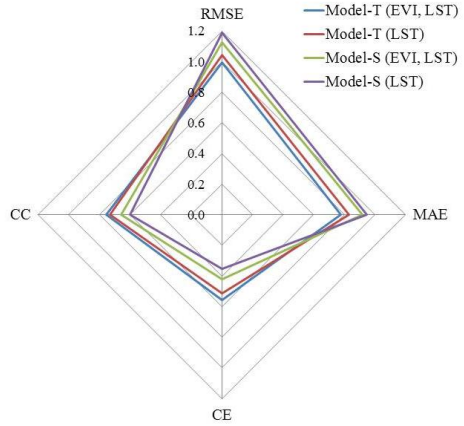

(a) Performance of individual models

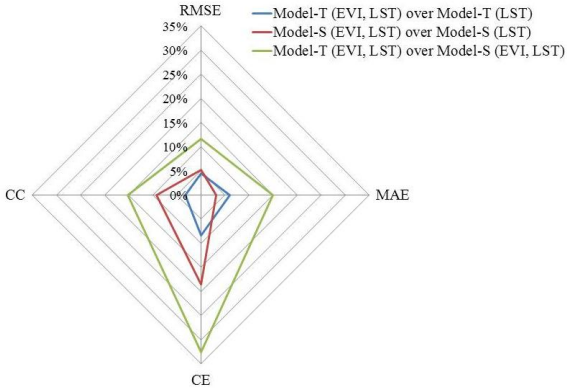

(b) Performance of Skill Score (SS)

Fig. 9. Performance comparison of the ANFIS models in testing phases w.r.t. different criteria (RMSE, MAE, CE, and CC).

HESSD
10, 6153–6192, 2013

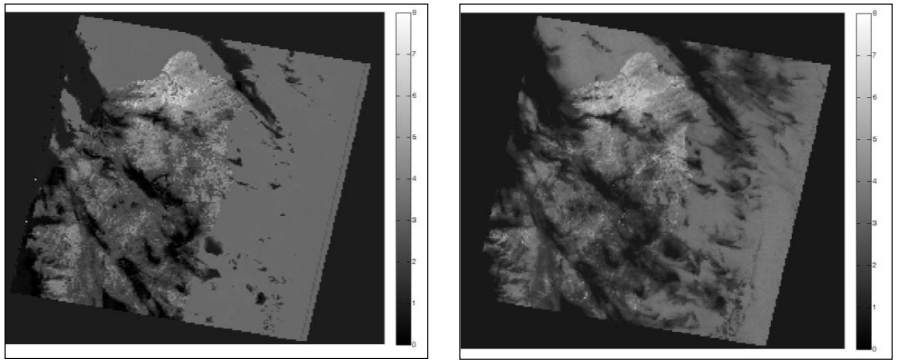

(a.1) Model-T(EVI, LST)

(a.2) Model-T (LST)

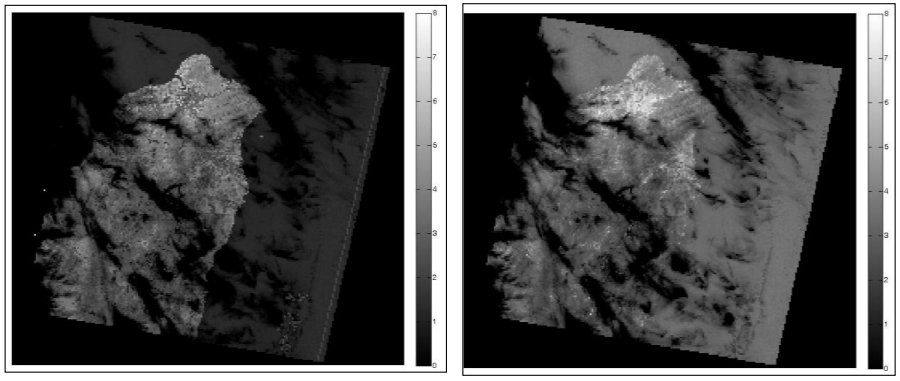

(b.1) Model-S(EVI, LST)

(b.2) Model-S(LST)

Fig. 10. Evaporation maps obtained from ANFIS models w.r.t different input combinations (evaporation unit: mm day^{-1}).

HESSD
10, 6153–6192, 2013

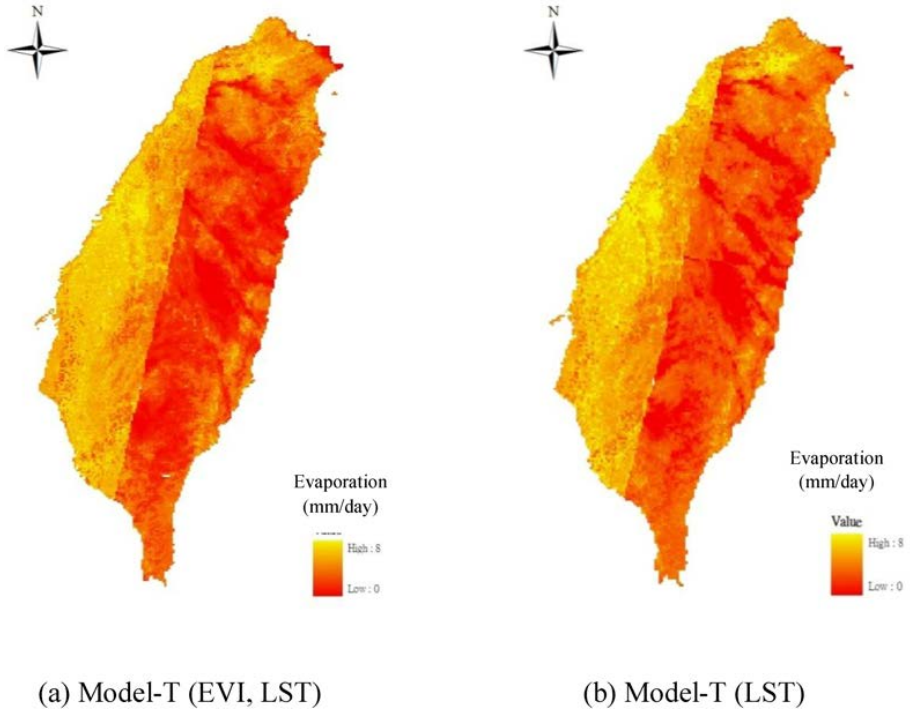

(a) Model-T (EVI, LST)

(b) Model-T (LST)

Fig. 11. Estimation of evaporation map for the whole Taiwan.

HESSD
10, 6153–6192, 2013